Mon. Not. R. Astron. Soc. **393,** 949–958 (2009) doi:10.1111/j.1365-2966.2008.14199.x

The Wouthuysen-Field effect in a clumpy intergalactic medium

Jonathan Higgins★ and Avery Meiksin
SUPA†, Institute for Astronomy, University of Edinburgh, Blackford Hill, Edinburgh EH9 3HJ

Accepted 2008 October 31. Received 2008 October 30; in original form 2008 July 7

ABSTRACT

We show that the high optical depth of the intergalactic medium to Lyα photons before the Epoch of Re-ionization results in a negligible magnitude for the Wouthuysen-Field effect produced by a radiation source on its distant surroundings, unless (i) the scattering medium has sufficient time for the impinging resonance line photons to establish a steady-state frequency distribution or (ii) the scattering gas is undergoing internal expansion or has a peculiar motion of tens to hundreds of km s^{-1} away from the source. Because of the intergalactic attenuation, discrete structures will receive only radiation from a source displaced from the resonance line frequency by typically hundreds to thousands of Doppler widths. The incident radiation must diffuse across the resonance line to produce a substantial scattering rate. We present steady-state solutions in the radiative diffusion approximation for the radiation field trapped in a clump of gas and show that this may result in an *enhancement* of the strength of the Wouthuysen-Field effect by as much as a factor of 10^6 over the free-streaming (single-scattering) limit. Solutions to the time-dependent diffusion equation, however, show that the time-scales required to establish a steady state will generally exceed the lifetime of the sources, resulting in a substantially reduced scattering rate. In the presence of internal expansion, a steady state may be established as photons are redshifted across the resonance line and into the red wing, and significant enhancement in the scattering rate over the free-streaming limit may again be produced. Alternatively, a substantial scattering rate may arise in systems with a peculiar motion away from the source that redshifts the received radiation into the resonance line centre. As a consequence, at epochs $z \lesssim 30$, when collisional decoupling of the hyperfine structure of hydrogen from the cosmic microwave background is small except in dense regions, and prior to the establishment of any large-scale diffuse radiation field of resonance line photons, the 21-cm signature from the intergalactic medium produced by the Wouthuysen-Field effect will, in general, trace the peculiar velocity field of the gas in addition to its density structure.

Key words: atomic processes – line: formation – radiative transfer – scattering – cosmology: theory – radio lines: general.

1 INTRODUCTION

Following the Recombination Era at $z \simeq 1100$, the baryons produced in the big bang were largely neutral. By $z \gtrsim 6$, the spectra of high-redshift quasi-stellar objects (QSOs) show that the hydrogen had become ionized (Becker et al. 2001). The history of structure formation in the wide redshift expanse between these epochs, when there were few if any sources of radiation, is largely unknown. In principle, 21-cm emission from the intergalactic hydrogen could reveal the evolution of structure in the baryons during these cosmic 'Dark Ages'. Because the baryons are cold, they would closely trace the evolution of the dark matter, so that 21-cm imaging could trace the growth of structure following the Recombination Era (Hogan & Rees 1979; Scott & Rees 1990). Because of strong coupling between the hyperfine structure of the hydrogen and the cosmic microwave background (CMB), however, a mechanism that decouples the spin temperature of the hydrogen hyperfine structure from the CMB temperature must be active, otherwise the hydrogen is rendered invisible: it absorbs and re-emits the CMB radiation at the same rate, leaving it indistinguishable from the CMB. At redshifts $z > 30$, collisions between hydrogen and electrons and other hydrogen atoms are adequate to begin decoupling the spin temperature from the CMB (Scott & Rees 1990; Madau, Meiksin & Rees 1997). Except in dense regions, however, at later times collisional decoupling is inadequate.

Once the first sources of radiation begin to turn on, the scattering of Lyα photons by the neutral hydrogen offers an alternative means of decoupling, through the Wouthuysen-Field effect (WFE)

★E-mail: jhi@roe.ac.uk
†Scottish Universities Physics Alliance.

(Wouthuysen 1952; Field 1958). As sources turn on in sufficient number to begin re-ionizing the intergalactic medium (IGM), they will produce a combined intensity of Lyα photons sufficient for coupling the spin temperature to the light temperature of the Lyα photons rather than the CMB, rendering the intergalactic hydrogen visible against the CMB in either emission or absorption (Madau et al. 1997).

The discovery of the End of the Dark Ages (EDA) and the onset of the Epoch of Re-ionization (EoR) have become one of the paramount goals of a new generation of radio telescopes, such as the LOw Frequency Array (LOFAR),[1] the Murchison Widefield Array (MWA),[2] the Primeval Structure Telescope/21 Centimeter Array (PaST/21CMA),[3] the Precision Array to Probe EoR (PAPER)[4] and a possible Square Kilometre Array (SKA).[5] Reviews of this rapidly growing area are provided by Loeb & Barkana (2001), Fan, Carilli & Keating (2006) and Furlanetto, Oh & Briggs (2006).

Madau et al. (1997) estimated the Lyα collision rate P_α that drives the WFE as the integrated intensity from cosmologically distributed sources, assuming that photons bluewards of Lyα emitted from a source will contribute their full amount to P_α once they redshift into the local Lyα resonance. In fact, this provides a lower limit (assuming photons are not destroyed by, e.g., dust absorption). The multiple scattering of resonance line photons will, in general, enhance the radiation field. For pure Doppler scattering, Field (1959a) argued that the rate is enhanced by the number of scatters a photon undergoes before being randomly scattered sufficiently redwards of line centre to escape. The estimate neglected scattering in the Lorentz wings, however. It also assumed that the IGM takes part in the homogeneous and isotropic expansion of the Universe. In fact, the IGM is clumpy, with structures breaking away from the cosmological expansion. Efforts are underway to estimate the radiation field and scattering rate in a cosmological context through Monte Carlo simulations of the scattering of resonance line photons in an inhomogeneous medium (Chuzhoy & Zheng 2007; Pierleoni, Maselli & Ciardi 2008; Semelin, Combes & Baek 2007). In this paper, we use analytical means to explore some of the consequences of intergalactic structure formation for the WFE as a means of generating an intergalactic 21-cm signature.

In the next section, we discuss the optical depth of the IGM to resonance line photons and the implications for the scattering rate. Approximate steady-state solutions to the radiative transfer equation are derived in Section 3 and time-dependent solutions in Section 4. A discussion of the solutions and applications is provided in Section 5, along with a summary of our conclusions.

2 THE WOUTHUYSEN-FIELD EFFECT IN THE INTERGALACTIC MEDIUM

The optical depth through a homogeneous and isotropic expanding IGM of a photon emitted by a source at redshift z_S and received at redshift z at frequency $\nu > \nu_0$, where ν_0 is the resonance line frequency, is (Field 1959a; Gunn & Peterson 1965)

$$\tau_\nu = \sigma \int_z^{z_S} \mathrm{d}z' \frac{\mathrm{d}l_p}{\mathrm{d}z'} n_1(z') \varphi_V\left(a, \nu \frac{1+z'}{1+z}\right), \quad (1)$$

where $n_1(z')$ is the number density of scattering atoms in the lower level at epoch z', $\sigma = \pi e^2 f_{lu}/(m_e c) \simeq 0.0110\,\mathrm{cm^2\,Hz}$ is the total resonance line cross-section, where $f_{lu} \simeq 0.4162$ is the upwards oscillator strength for hydrogen Lyα, $\varphi_V(a, \nu)$ is the Voigt line profile normalized to $\int \mathrm{d}\nu \varphi_V(a, \nu) = 1$, $a \simeq 0.0472 T^{-1/2}$ is the ratio of the decay rate to the Doppler width $\Delta\nu_D = \nu_0 b/c$, where $b = (2k_B T/m_H)^{1/2}$ is the Doppler parameter for hydrogen gas at temperature T and c is the speed of light and l_p is the proper path length. In the Lorentz wing, expressed as a function of $x = (\nu - \nu_0)/\Delta\nu_D$, the dimensionless Voigt profile $\phi_V(a, x) = (\Delta\nu_D)\varphi_V(a, \nu)$ is well approximated as $\phi_V(a, x) \simeq a/(\pi x^2)$. The differential proper line element evolves according to $\mathrm{d}l_p/\mathrm{d}z \simeq (c/H_0)\Omega_m^{-1/2}(1+z)^{-5/2}$ in a flat universe at redshifts for which $\Omega_m(1+z)^3$ dominates the contribution from the vacuum energy, where Ω_m is the ratio of the total mass density to the critical Einstein–de Sitter density, and where $H_0 = 100\,h\,\mathrm{km\,s^{-1}\,Mpc^{-1}}$ is the Hubble constant today.

Photons emitted by the source at a frequency $\nu_e > \nu_0(1+z_S)/(1+z)$ will scatter in the blue Lorentz wing (except for those for which the inequality is nearly an equality, in which case they will scatter through the Doppler core). In the blue wing, the optical depth due to Lyα scattering by neutral hydrogen is

$$\tau_\nu \simeq 1.75 \times 10^5 \frac{c n_1(0)}{H_0 \Omega_m^{1/2}} \frac{(1+z)^{3/2}}{\nu_0^2 y^{3/2}} \left\{ \left[\frac{y^{1/2}}{y-1} - \frac{u^{1/2}}{u-1} \right] + \frac{1}{2} \log \left[\frac{(1-u^{1/2})(1+y^{1/2})}{(1-y^{1/2})(1+u^{1/2})} \right] \right\}, \quad (2)$$

where $y = \nu/\nu_0$ and $u = y(1+z_S)/(1+z)$, and all quantities are assumed to be in cgs units. For $0 < xb/c \ll (z_S - z)/(1+z) \ll 1$, the expression simplifies to

$$\tau_\nu \approx \frac{x_1}{x}, \quad (3)$$

where

$$x_1 = \frac{a}{\pi} \frac{\sigma c}{\nu_0} \frac{n_1(0)}{H_0 \Omega_m^{1/2}} (1+z)^{3/2} \approx 214 h^{-1} (1+z)^{3/2} T_{IGM}^{-1/2} \quad (4)$$

for a mean line-of-sight IGM temperature T_{IGM} for a universe with $\Omega_m = 0.3$ and baryon density $\Omega_b h^2 = 0.022$ (O'Meara et al. 2006; Spergel et al. 2007). As an illustration, $\tau_\nu(x)$ for a source at $z_S = 8$ is shown at $z = 7$ in Fig. 1 (upper panel). The optical depth is extremely high until ν is well displaced from the line centre. The values of x_1, at which $\tau_\nu = 1$, are shown in the lower panel of Fig. 1 for a range of redshifts.

Photons emitted by the source with frequencies between $\nu_0 < \nu_e < \nu_0(1+z_S)/(1+z)$ will pass through the resonance line frequency en route to the gas at z. Upon passing through the resonance line, the photons will essentially be completely scattered out of the line of sight. As a consequence, essentially no photons will be received in the frequency range $\nu_0(1+z)/(1+z_S) < \nu < \nu_0$ (the Gunn–Peterson effect). A general expression for the optical depth through the Doppler core is provided in Appendix A.

Photons emitted sufficiently redwards of ν_0 to avoid the Doppler core may still be scattered in the Lorentz red wing of the surrounding hydrogen. This will produce a halo of scattered Lyα photons around a central source like a QSO (Loeb & Rybicki 1999). For frequencies $x < 0$ near line centre, Loeb & Rybicki (1999) show that the photons will build up an energy density as they diffuse through the surrounding IGM of the form $u_\nu \sim (-x)^{-9/2} e^{-[r/r_c(x)]^2}$, where $r_c(x) = (-x)^{1/2}\ (2/3)[(b/H)\lambda_{mfp}(x)]^{1/2}$ scales like the harmonic mean between the distance over which Hubble expansion

[1] www.lofar.org
[2] www.haystack.mit.edu/ast/arrays/mwa
[3] web.phys.cmu.edu/∼past
[4] astro.berkeley.edu/∼dbacker/eor
[5] www.skatelescope.org

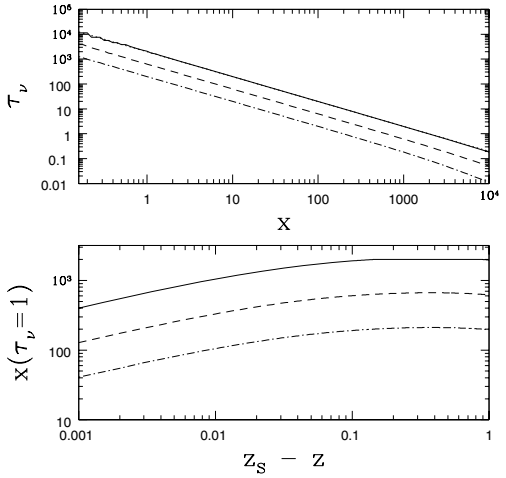

Figure 1. Upper panel: the optical depth of photons emitted by a source at redshift z_S and received at the frequency ν near the resonance line frequency ν_0 of Lyα at redshift z. The frequency is expressed as $x = (\nu - \nu_0)/\Delta\nu_D$. The curves are for $T = 10$ K (solid), 100 K (dashed) and 1000 K (dot-dashed). Also shown is the approximation $\tau_\nu \simeq x_1/x$ for the $T = 10$ K model (dotted line, nearly coinciding with the solid line). Lower panel: the value of x at which $\tau_\nu = 1$ for $z_S - 1 < z < z_S$. The curves are labelled as in the upper panel.

produces a velocity difference matching the Doppler parameter b and the scattering mean-free path of a resonance line photon in the Lorentz wing

$$\lambda_{\rm mfp}(x) \simeq \frac{\pi\Delta\nu_D}{n_1\sigma a}x^2, \tag{5}$$

where n_1 is the number density of atoms in the lower level. The energy density is exponentially suppressed for $x \to 0^-$ at a fixed position, resulting in a negligible Lyα scattering rate except very near the QSO. Numerically,

$$r_c(x) \simeq 0.6\,{\rm pc}(-x)^{3/2}h^{-1/2}T_{\rm IGM}^{3/4}\Omega_{\rm m}^{-1/4}\left(\frac{1+z}{9}\right)^{-9/4}, \tag{6}$$

so that a substantial Lyα scattering rate is confined to a small region around the source. The region is so small in fact that the assumption that the surrounding IGM takes part in the Hubble flow will not be valid. More likely, the gas would have been ionized and violently disturbed by the QSO itself.

Finally, photons emitted sufficiently redwards of ν_0 at the source to escape scattering in the Lorentz wing will pass freely through the IGM, where they will be received at redshift z at frequencies $x < -x_0$, where

$$x_0 = \frac{c}{b_{\rm IGM}}\frac{z_S - z}{1+z_S} \simeq 2.3\times10^6 T_{\rm IGM}^{-1/2}\frac{z_S - z}{1+z_S}. \tag{7}$$

The vast majority of photons from the source emitted bluewards of, but near, the resonance line frequency never arrive near the line centre, having been scattered out of the path along the way. The resonance line radiation impinging on the absorption site[6] from the source scatters in the Lyα resonance line at the rate per neutral atom in the lower state

$$P_1 = \sigma c\int_0^\infty {\rm d}\nu\varphi_V(a,\nu)\frac{u_\nu}{h_P\nu}, \tag{8}$$

where h_P is Planck's constant and u_ν is the local specific energy density of photons received at z from the source at z_S with specific luminosity L_ν

$$u_\nu = \frac{1}{c}\frac{L_\nu}{4\pi r_L^2}\exp(-\tau_\nu), \tag{9}$$

where r_L is the luminosity distance between the source and the gas at redshift z. The scattering rate assuming none of the photons has been scattered out of the line of sight en route to the absorption site (the free-streaming limit) is

$$P_1(\tau_\nu = 0) \simeq \sigma\frac{L_\nu/h_P\nu}{4\pi r_L^2}. \tag{10}$$

The ratio of the scattering rate for $\tau_\nu \simeq x_1/x$ to the free-streaming value is then given by

$$\frac{P_1(\tau_\nu)}{P_1(\tau_\nu=0)} \simeq \frac{\int_0^\infty {\rm d}x a\pi^{-1}x^{-2}\exp(-x_1/x)}{\int_{-\infty}^\infty {\rm d}x\phi_V(a,x)} = \frac{a}{\pi x_1}$$
$$\simeq 7.0\times10^{-5}h(1+z)^{-3/2}\left(\frac{T_{\rm IGM}}{T_a}\right)^{1/2}, \tag{11}$$

where T_a is the temperature of the absorbing gas. The low value poses a fundamental problem to the effectiveness of the WFE as a means of decoupling the spin state of the gas from statistical equilibrium with the CMB. *Only if photons have sufficient time to diffuse across the line centre will the scattering of Lyα photons be an effective means of decoupling the spin temperature from the CMB in comoving objects.*

3 THE WOUTHUYSEN-FIELD EFFECT IN DISCRETE OBJECTS

3.1 Steady-state solutions without atomic recoil

The assumption of a homogeneous and isotropic universe, while a fair approximation over large scales, breaks down on small scales: the IGM is clumpy at the redshifts from which the 21-cm signal is expected (Tozzi et al. 2000; Gnedin & Shaver 2004). For a sufficiently short mean-free path, photons will be trapped within a discrete system and diffuse in frequency and space as they scatter within the system. In this section, we consider the energy distribution the radiation will reach given an adequate time to relax to a steady state.

For a Lyα photon to become trapped within an absorber of length-scale L_a, the mean-free path must minimally satisfy $\lambda_{\rm mfp} < L_a$, for which $\tau_\nu = L_a/\lambda_{\rm mfp} > 1$. As the optical depth in the wing may be expressed as $\tau_\nu = \pi^{-1/2}(a\tau_0)x^{-2}$, where $\tau_0 = n_1L_a\pi^{-1/2}\sigma(\Delta\nu_D)^{-1}$ is the optical depth at the line centre, this corresponds to photons escaping with $x > \pi^{-1/4}(a\tau_0)^{1/2}$ (Osterbrock 1962). Radiative transfer solutions for sources embedded within a slab suggest that this may be somewhat too restrictive for systems with very high line centre optical depths, in which case the photons escape through spatial diffusion rather than frequency diffusion. Steady-state solutions in the diffusion approximation for scattering in the Lorentz wings in very high optical depth systems show that photons escape the slabs with frequencies typically of the order of $(a\tau_0)^{1/3}$ (Adams 1972; Harrington 1973; Neufeld 1990). An escape frequency of $x_{\rm esc} = x_*(a\tau_0)^{1/3}$ corresponds to a mean-free path smaller than the thickness of the slab by a factor of $f = x_*^2\pi^{1/2}\,(a\tau_0)^{-1/3} \simeq 0.013x_*^2T_a^{1/3}$

[6] Strictly speaking, the photons are scattered. The region at which the scattering rate is computed is referred for simplicity as the absorption site or the absorber.

$N_{19}^{-1/3}$, where T_a is the temperature of the absorber and N_{19} is the column density in units of 10^{19} cm^{-2}. (This corresponds to a region 24 kpc across for the mean intergalactic hydrogen density at $z = 8$, and smaller for overdense systems.) As f depends only weakly on T_a and N_{H1}, while x_* depends on $a\tau_0$ and the radiation source parameters of any particular problem, we express the escape frequency simply as

$$x_{esc} \simeq 395(10f)^{1/2} N_{19}^{1/2} T_a^{-1/2}, \tag{12}$$

noting that f will, in general, vary with the depth within the absorber, and must be solved for according to each particular configuration, but will be of the order of 0.01–1 for applications we consider. Comparison of equation (12) with equation (4) for x_1 shows that photons with $\tau_\nu < 1$ in the IGM will not generally be trapped within a structure comoving with the expansion of the Universe unless the structure has a neutral hydrogen column density $N_{19} > N_{19,crit}$, where

$$N_{19,crit} \simeq 0.29\, h^{-2} (10f)^{-1} (1+z)^3 \left(\frac{T_a}{T_{IGM}}\right). \tag{13}$$

If $x_1 < x_{esc}$, the absorber will behave as a photon bucket, allowing the energy density of the radiation field at frequencies $x < x_{esc}$ to build up with time as radiation from the source becomes trapped. As the photons scatter within the absorber, they will diffuse in frequency and space. Because photons with $|x| > x_{esc}$ will escape, the energy density of the radiation trapped within the absorber will reach a steady state when the rate of incoming photons balances the rate of escape. In principle, the energy density that develops could produce a substantial scattering rate, even exceeding the rate estimated assuming no photon losses from the source due to scattering by the intervening IGM.

The depth to which photons at frequency x_1 penetrate an absorber depends on the optical depth of the absorber. If it is optically thin at x_1, the photons will stream through. If optically thick, the photons will scatter near the surface of the absorber. Photons bluewards of x_1, however, will penetrate more deeply, as the cross-section diminishes like $1/x^2$. In general, photons will be injected at varying layers within the absorber, with bluer photons injected at increasing depths.

We would like to estimate the evolution of the radiation field within an absorber. No solution to this problem exists in the literature. The full radiative transfer problem through the slab is an involved one, as the radiation field will vary with both the optical depth through the slab and with frequency. It is particularly important in our application to obtain the solution across the Doppler core to estimate the Lyα scattering rate. Instead of solving the full problem, we seek approximate solutions in which we treat the scattered radiation field as locally isotropic, neglecting the spatial diffusion of the radiation through the absorber. We show in Appendix B that the resulting radiative transfer equation in the diffusion approximation is formally identical to the equation of Harrington (1973) for the problem of a slab with a uniform distribution of spectrally flat sources. The solution we obtain neglecting the spatial diffusion of the radiation agrees well with Harrington's solution which includes both spatial and frequency diffusion. A detailed quantitative description will require a more exact solution to the problem, but our approximate approach allows us to explore qualitatively several effects of interest. We would like to estimate the energy density that may be achieved as a function of x_{esc}. We also wish to examine the effect of internal motions on the radiation energy density across the line centre and the possible role of atomic recoil. Lastly, we would like to estimate the time it takes for the radiation field to establish a steady state. All of these effects extend well beyond those explored by existing slab solutions.

We estimate the radiation density that builds up within an absorber by assuming a steady state between the rate of photons injected into the absorber and the rate of diffusion of the photons across the escape frequency, imposing the boundary condition $u(x) = 0$ for $|x| > x_{esc}$, where $u(x) = \Delta\nu_D u_\nu$. We assume isotropic scattering within a homogeneous absorber and use the diffusion approximation to describe the resonance line scattering of the photons. In equilibrium,

$$\frac{1}{2}\frac{d}{dx}\left[D(a,x)\frac{dn(x)}{dx}\right] = -\tilde{S}(x), \tag{14}$$

where $n(x) = \Delta\nu_D n_\nu$, $n_\nu = u_\nu/h_P\nu$, $\tilde{S}(x) = (\Delta\nu_D)^2 S(\nu)/(n_I c\sigma)$, where $S(\nu)$ is a source function, and $D(a, x)$ is the diffusion coefficient. The second-order moment of the frequency redistribution function gives for the diffusion coefficient $D(a, x) = \phi_V(a, x) + (1/3)d^2\phi_V(a, x)/dx^2$ (Rybicki & dell'Antonio 1994). The derivation of the diffusion equation, however, does not conserve photon number to the order of the approximation. As a consequence, the diffusion coefficient is left ambiguous. Rybicki & dell'Antonio (1994) advocate adopting $D(a, x) = \phi_V(a, x)$ for its simplicity, and we will do so here.

The source $S(\nu)$ represents the rate at which photons received from the source are incident on the absorber at $x < x_{esc}$, where they are trapped and diffuse in frequency. It is given by the scattering emissivity (per photon energy)

$$S(\nu) = n_I c\sigma \int_0^\infty d\nu' R(\nu', \nu) n_{\nu'}, \tag{15}$$

where $R(\nu', \nu)$ is the photon redistribution function for resonance line scattering (Mihalas 1978). Since scattering in the wings is coherent, $R(\nu', \nu) \simeq \varphi_V(a, \nu')\delta_D(\nu' - \nu)$, where δ_D is the Dirac δ function. Then,

$$\begin{aligned} S(\nu) &\simeq n_I c\sigma \varphi_V(a, \nu) n_\nu \\ &\simeq n_I \sigma a \pi^{-1} (\Delta\nu_D)^{-1} \frac{L_\nu/h_P\nu}{4\pi r_L^2} x^{-2} \exp(-x_1/x). \end{aligned} \tag{16}$$

The dependence on x results in a sharp peak at $x = x_1/2$, so that the source $\tilde{S}(x)$ is well approximated by

$$\begin{aligned} \tilde{S}(x) &\simeq \frac{a}{\pi c}\frac{\Delta\nu_D}{x_1}\frac{L_\nu/h_P\nu}{4\pi r_L^2}\delta_D(x - x_{inj}) \\ &= A\delta_D(x - x_{inj}), \end{aligned} \tag{17}$$

where the normalization constant $A = 2.5 \times 10^{-6} h (1+z)^{-3/2} T_{IGM}^{1/2}$ $[(L_\nu/h_P\nu)/4\pi r_L^2]$ (with all quantities expressed in cgs units), matches the source rate of equation (16) integrated over all frequencies. Note that the dependence on the absorber temperature cancels. Here, the frequency at which photons are injected into the absorber is represented generally as x_{inj} to allow for any peculiar motion of the absorber, which could shift the peak of the received radiation either redwards or bluewards, and to allow for scattering within the absorber which will shift the peak of the radiation field penetrating to deeper layers further towards the blue. For a comoving absorber, $x_{inj} = x_1/2$ near the surface. The solution to equation (14) using the wing approximation for $\phi_V(a, x)$ is

$$n(x) = \begin{cases} \frac{\pi}{3a} A \left(1 - \frac{x_{inj}^3}{x_{esc}^3}\right)\left(x_{esc}^3 + x^3\right) & ; -x_{esc} < x < x_{inj} \\ \frac{\pi}{3a} A \left(1 + \frac{x_{inj}^3}{x_{esc}^3}\right)\left(x_{esc}^3 - x^3\right) & ; x_{inj} < x < x_{esc}. \end{cases} \tag{18}$$

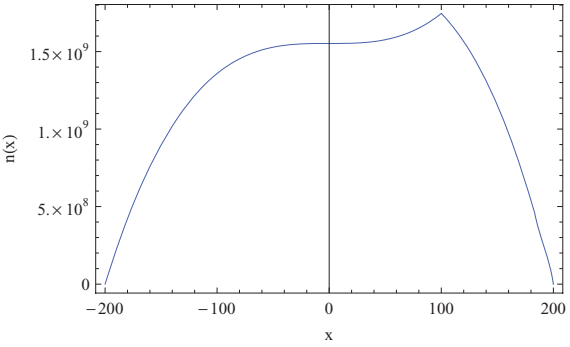

Figure 2. The steady-state distribution of Lyα resonance line photons for a source function $\tilde{S}(x) = \delta_{\rm D}(x - x_{\rm inj})$ with $x_{\rm inj} = 100$, allowing photons with $|x| > x_{\rm esc} = 200$ to escape, as given by the diffusion approximation, equation (14), with $D(a, x) = \phi_{\rm V}(a, x)$. An absorber temperature $T_{\rm a} = 100$ K is assumed.

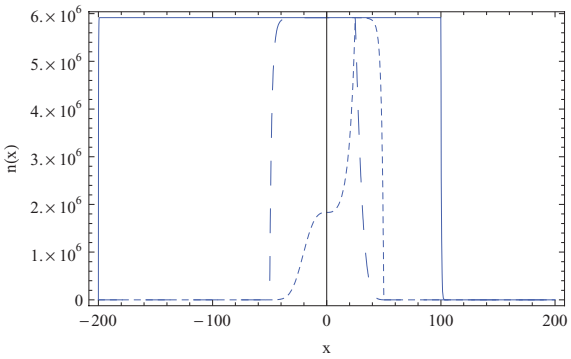

Figure 3. The steady-state distribution of Lyα resonance line photons for a source function $\tilde{S}(x) = \delta_{\rm D}(x - x_{\rm inj})$ with $x_{\rm inj} = 100$ in an absorber with temperature $T_{\rm a} = 100$ K, allowing photons with $|x| > x_{\rm esc} = 200$ to escape and including the effects of internal motions with a dimensionless velocity gradient $\gamma = 1.7 \times 10^{-7}$ (solid line), representing expansion. Virtually all the injected photons are redshifted, escaping for $x < -x_{\rm esc}$. The solution for $x_{\rm inj} = 25$ and $x_{\rm esc} = 50$ for $\gamma = 1.7 \times 10^{-7}$ is also shown (long-dashed line), showing a weak tail at $x > x_{\rm inj}$. The corresponding case with contraction, $\gamma = -1.7 \times 10^{-7}$ (short-dashed line) shows a more complex behaviour as contraction curtails the redwards diffusion.

The solution is shown in Fig. 2. We find that adopting $D(a, x) = \phi_{\rm V}(a, x) + (1/3)d^2\phi_{\rm V}(a, x)/{\rm d}x^2$ produces a nearly identical solution, agreeing to within a fraction of a per cent for $x_{\rm inj}$ well out of the core. Numerically integrating the diffusion equation using the full Voigt profile produces a solution that also differs negligibly from equation (18).

The ratio of the collision rate $P_{\rm l}$, given by using equation (18) in equation (8), to the free-streaming collision rate $P_{\rm l}(0)$ of equation (10) is then

$$\begin{aligned}\frac{P_{\rm l,ss}}{P_{\rm l}(0)} &\simeq \frac{1}{x_1}\frac{a}{\pi A}\int_{-\infty}^{\infty}{\rm d}x\,\phi_{\rm V}(a,x)n(x)\\ &\simeq \frac{1}{3x_1}\left[\left(1-\frac{x_{\rm inj}^3}{x_{\rm esc}^3}\right)x_{\rm esc}^3+\frac{a}{\pi}\left(3x_{\rm inj}^2-x_{\rm esc}^2-2\frac{x_{\rm inj}^3}{x_{\rm esc}}\right)\right]\\ &\simeq \frac{1}{3x_1}\left(1-\frac{x_{\rm inj}^3}{x_{\rm esc}^3}\right)x_{\rm esc}^3\\ &\simeq 9.6\times10^4 h\left[\frac{(10f)N_{19}}{(1+z)T_{\rm a}}\right]^{3/2}T_{\rm IGM}^{1/2}\left(1-\frac{x_{\rm inj}^3}{x_{\rm esc}^3}\right),\end{aligned}\qquad(19)$$

where we have used the approximation equation (A1) for the Voigt profile with $x_{\rm esc} > x_{\rm inj} \gg x_m$ assumed, and neglected the terms following the leading. The enhancement may be substantial. For $N_{19} = N_{19,\rm crit}$, $P_{\rm l,ss}/P_{\rm l}(0) \simeq 1.5\times10^4 h^{-2}(1+z)^3 T_{\rm IGM}^{-1}(1-x_{\rm inj}^3/x_{\rm esc}^3)$, so that even for a warm IGM temperature of $T_{\rm IGM} = 1000$ K, a substantial boost in the scattering rate will result.

The solution equation (18) assumes that velocities internal to the cloud are negligible. To estimate the effect internal motion may have on the frequency distribution of the photons, we approximate the motion as an isotropic expansion (or contraction) within the cloud characterized by a uniform velocity gradient $H_{\rm a}$ (which, in general, will not be the same as the Hubble parameter). In the diffusion approximation, equation (14) is modified to (Rybicki & dell'Antonio 1994)

$$\frac{1}{2}\frac{\rm d}{{\rm d}x}\left[2\gamma n(x) + D(a,x)\frac{{\rm d}n(x)}{{\rm d}x}\right] = -\tilde{S}(x),\qquad(20)$$

where $\gamma = \nu_0 H_{\rm a}/(\sigma n_{\rm l} c)$ is (c/b) times the ratio of the scattering time of the photons at line centre to the expansion time $H_{\rm a}^{-1}$ of the gas. For this solution, the steady state applies to the comoving number density of photons per frequency (Rybicki & dell'Antonio 1994). Overdense structures are typically contracting, but the internal motions along a filament may expand along the filament in regions (Zhang et al. 1998). For an overdensity 10 times the cosmic mean at $z = 8$, an internal velocity gradient of 100 km s^{-1} over 100 kpc corresponds to $\gamma \simeq 1.7 \times 10^{-7}$. Contraction by the same magnitude corresponds to $\gamma \simeq -1.7 \times 10^{-7}$.

The solution for the source $\tilde{S}(x) = A\delta_{\rm D}(x - x_{\rm inj})$ is

$$n(x) = \begin{cases} g_\gamma(x, -x_{\rm esc}) & ; -x_{\rm esc} < x < x_{\rm inj} \\ g_\gamma(x, -x_{\rm esc}) - g_\gamma(x, x_{\rm inj}) & ; x_{\rm inj} < x < x_{\rm esc} \end{cases},\qquad(21)$$

where $g_\gamma(x, y) = (A/\gamma)f_\gamma(x_{\rm esc}, x_{\rm inj})f_\gamma(x, y)/f_\gamma(x_{\rm esc}, y)$ and $f_\gamma(x, y) = 1 - \exp[-\frac{2\pi\gamma}{3a}(x^3 - y^3)]$. The solution is extremely sensitive to $\gamma x_{\rm esc}^3/a$. For $\gamma \gg \gamma_{\rm crit} \equiv 3a/(2\pi\, x_{\rm esc}^3)$, a broad wing of amplitude A/γ redwards of $x_{\rm inj}$ will result as photons are redshifted across the line centre. The distribution will cut-off sharply at $x > x_{\rm inj}$. For an absorber with $T_{\rm a} = 100$ K ($a \simeq 0.00472$) and $x_{\rm esc} = 200$, $\gamma_{\rm crit} \simeq 2.8 \times 10^{-10}$. The solutions for $\gamma = 1.7 \times 10^{-7}$ with $(x_{\rm inj}, x_{\rm esc}) = (100, 200)$ and $(25, 50)$ are shown in Fig. 3. A substantial decrease in $n(x)$ is produced compared with the $\gamma = 0$ case. A significant enhancement of the Lyα collision rate over the free-streaming limit, however, may still result, with $P_{\rm l,ss}/P_{\rm l}(0) \simeq a/(\pi\gamma x_1)$. For $\gamma < 0$, a broad wing bluewards of $x_{\rm inj}$ will form as photons are blueshifted in the contracting gas. A complex profile, however, may form redwards of $x_{\rm inj}$ as redward diffusion is resisted by blueshifting. Such a case is illustrated in Fig. 3 for $\gamma = -1.7 \times 10^{-7}$ with $x_{\rm inj} = 25$ and $x_{\rm esc} = 50$.

3.2 Steady-state solution with atomic recoil

The above solutions neglect the effect of atomic recoil on the evolution of the radiation field. Since the photon momentum ($\sim h_{\rm P}\nu_0/c$) is small as compared to the momentum of the hydrogen atoms ($\sim m_{\rm H} b$), the effect should be small, but may result in a significant heating rate when the gas is still cold (Madau et al. 1997; Chen & Miralda-Escudé 2004; Meiksin 2006). Allowing for atomic recoils modifies equation (14) to

$$\frac{1}{2}\frac{\rm d}{{\rm d}x}\left[2\epsilon\phi_{\rm V}(a,x)n(x) + D(a,x)\frac{{\rm d}n(x)}{{\rm d}x}\right] = -\tilde{S}(x),\qquad(22)$$

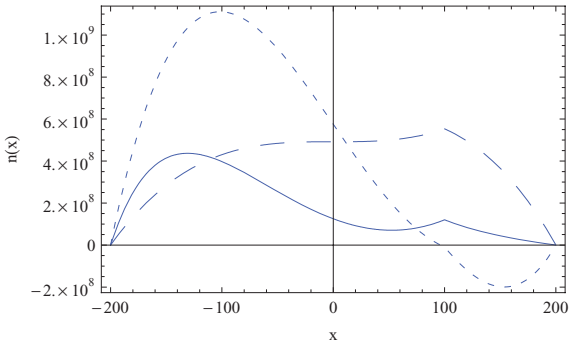

Figure 4. The steady-state distribution of Lyα resonance line photons in the diffusion approximation for a source function $\tilde{S}(x) = \delta_{\rm D}(x - x_{\rm inj})$ with $x_{\rm inj} = 100$, allowing photons with $|x| > x_{\rm esc} = 200$ to escape and including the effect of atomic recoils. Shown are the solution with $\epsilon = 0.0079$, corresponding to $T_{\rm a} = 10$ K (solid line), the solution with $\epsilon = 0$ (long-dashed line) and the first-order solution $n_0(x) + \epsilon n_1(x)$ for $\epsilon = 0.0079$ (short-dashed line).

where the recoil parameter $\epsilon = h_{\rm P}\nu_0/(2k_{\rm B}Tm_{\rm H}c^2)^{1/2} \simeq 0.025T^{-1/2}$ is the ratio of the momentum of a resonance line photon to the momentum of an atom moving at the thermal velocity (Rybicki & dell'Antonio 1994; Meiksin 2006). Equation (22) expresses only the first-order correction in ϵ. The solution for a source $\tilde{S}(x) = A\delta_{\rm D(}x - x_{\rm inj})$ is

$$n(x) = \begin{cases} g_\epsilon(x, -x_{\rm esc}) & ; -x_{\rm esc} < x < x_{\rm inj} \\ g_\epsilon(x, -x_{\rm esc}) - g_\epsilon(x, x_{\rm inj}) & ; x_{\rm inj} < x < x_{\rm esc}, \end{cases} \quad (23)$$

where $g_\epsilon(x, y) = A[\pi/(2\epsilon^3\, a)]\, \exp(-2\epsilon x)[f_\epsilon(x) - f_\epsilon(y)][f_\epsilon(x_{\rm esc}) - f_\epsilon(x_{\rm inj})]/[f_\epsilon(x_{\rm esc}) - f_\epsilon(y)]$ and $f_\epsilon(x) = (1 - 2\epsilon x + 2\epsilon^2 x^2)\, \exp(2\epsilon x)$. Here, the wing approximation for $\phi_{\rm V}(a, x)$ is adopted, but we find a nearly identical result allowing for the Doppler core as well.

The solution for $x_{\rm inj} = 100$, $x_{\rm esc} = 200$ and $\epsilon = 0.0079$, corresponding to $T \simeq 10$ K, is shown in Fig. 4. The result differs substantially from the solution for $\epsilon = 0$. In fact, the solution cannot be trusted, as it is not consistent with the original order of equation (22) in ϵ. This may be demonstrated by adding the quantity $\epsilon^2 y(x)$ to $2\epsilon\phi_{\rm V}(a, x)n(x)$, where $y(x)$ is an unspecified function representing the higher order corrections to the recoil, and which, in general, may also depend on $n(x)$. Inserting the series solution $n(x) = \Sigma_{i=0}^{\infty}\epsilon^i n_i(x)$ into equation (22) and equating equal orders in ϵ recovers $n_0(x)$ as given by equation (18) and produces the first-order equation $({\rm d}/{\rm d}x)[2\phi_{\rm V}(a, x)n_0(x) + D(a, x)\, {\rm d}n_1(x)/{\rm d}x] = 0$ and the second-order equation $({\rm d}/{\rm d}x)[2\phi_{\rm V}(a, x)n_1(x) + y(x) + D(a, x)\, {\rm d}n_2(x)/{\rm d}x] = 0$. The first-order equation gives $n_1(x)$ in terms of $n_0(x)$, subject to the boundary conditions $n_1(-x_{\rm esc}) = n_1(x_{\rm esc}) = 0$. The second-order equation shows that $n_2(x)$ depends on the unspecified (neglected) function $y(x)$. Thus, the solution is valid only up to $n(x) = n_0(x) + \epsilon n_1(x)$. If higher order terms are substantial, then the solution for $n(x)$ cannot be trusted. The solution $n_0(x) + \epsilon n_1(x)$ for the above example differs substantially from the solution $n(x)$, and indeed is not even positive definite, as shown in Fig. 4, demonstrating the solution is not valid.

Including higher order terms involves a non-trivial expression for the redistribution function including non-linear terms in the recoil parameter (Basko 1981; Meiksin 2006). (Additional higher order terms in the recoil parameter arise from relativistic corrections, but these are reduced by factors of b/c.) For temperatures $T > 100$ K, the discrepancy between the full solution and the first-order solution is smaller than about 20 per cent for $x_{\rm inj} = 100$ and $x_{\rm esc} = 200$. In general, the correction will be small for $\epsilon x_{\rm esc} \ll 1$, and we caution that if this is violated then the steady-state solutions may not be valid. We do not pursue further consequences of the atomic recoil solution here.

3.3 The role of bulk peculiar velocities

Absorption systems with a bulk peculiar velocity component away from the source will see the photons redshifted into line centre. In this case, the scattering rate of resonance line photons may be appreciable even in an optically thin absorber ($N_{19} < N_{19,\rm crit}$), so that the buildup of a strong radiation field at line centre through photon capture and diffusion is not necessary for significant WFE decoupling of the spin state from the CMB. The peculiar velocity required to bring the absorber into the peak of the source function $S(\nu)$ in equation (16) is given by $v_{\rm pec} \simeq \frac{1}{2}x_1 b_{\rm a}$, where x_1 is given by equation (4). For pure thermal broadening (assuming negligible internal velocity structure within the absorber), this corresponds to

$$v_{\rm pec} \simeq 14h^{-1}(1+z)^{3/2}\left(\frac{T_{\rm a}}{T_{\rm IGM}}\right)^{1/2}\ {\rm km\,s^{-1}}. \quad (24)$$

This is comparable to the typical peculiar velocities of non-linear cosmological structures at the epochs of interest. As a result, *the WFE will produce a 21-cm signature that maps the peculiar velocity field of the structures within the IGM*.

As an illustration, we consider the signal produced by a collapsing halo, such as around a forming galaxy or galaxy cluster, illuminated by an external radiation source, as depicted in Fig. 5.

The collision rate from a source of specific luminosity L_ν on an absorber with Doppler parameter $b_{\rm a}$ at luminosity distance $r_{\rm L}$ moving away from the source with peculiar velocity v is

$$P_{\rm l} = \sigma\frac{L_\nu}{h_{\rm P}\nu}\frac{1}{4\pi r_{\rm L}^2}\int_0^\infty {\rm d}\nu\, \varphi_{\rm V}\left[a, \nu\left(1 - \frac{v}{c}\right)\right]\exp(-\tau_\nu)$$
$$\simeq \sigma\frac{L_\nu}{h_{\rm P}\nu}\frac{1}{4\pi r_{\rm L}^2}\exp\left[-\frac{b_{\rm a}x_1}{v_0\cos(\theta)}\right], \quad (25)$$

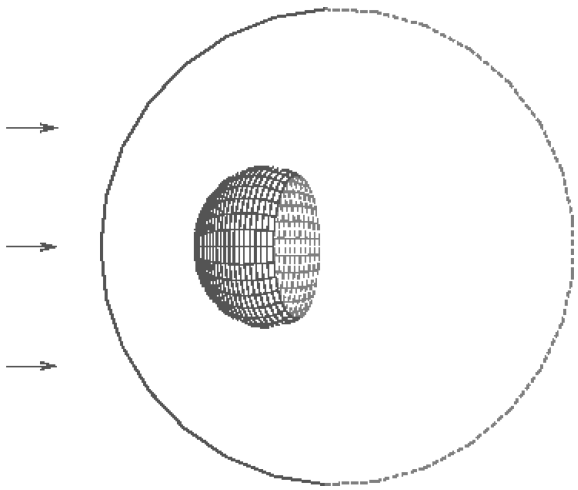

Figure 5. Surface of constant Lyα scattering rate $P_{\rm l}$ produced by a continuum source to the left within a collapsing halo of neutral hydrogen. The inner surface terminates at the accretion shock. The circle represents the turnaround radius $r_{\rm ta}$ of the halo, with the solid line representing the hemisphere of gas with peculiar velocity redshifted relative to the source and the dashed line the hemisphere with blueshifted peculiar velocity. The surface shown corresponds to a maximum radius of $0.59r_{\rm ta}$. The figure is tilted by 5° to reveal the three-dimensional structure of the surface.

using equation (3), approximating $\phi_V(a, x) \simeq \pi^{-1/2} \exp(-x^2)$, noting that the resulting exponential in the integrand peaks sharply near $x = v/b_a$ assuming $v_0/b_a \simeq x_1$ or larger, Taylor expanding the argument of the exponential to second order in $x - v/b_a$ and expressing the peculiar velocity as $v = v_0 \cos(\theta)$, the projected accretion velocity along the line of sight to the source.

In general, v_0 will vary with distance from the centre of the collapsing halo. As a definite case, we approximate the peculiar velocity of the accreting gas using the self-similar solution of Bertschinger (1985) for the adiabatic accretion of a $\gamma = 5/3$ gas of negligible density on to a dark matter halo with a comoving centre in an Einstein–de Sitter cosmology. The velocity field in the region between the accretion shock and the turn-around radius at cosmological time t is well approximated by

$$v_0(r) \simeq \frac{r_{ta}}{t} \frac{V_{min}}{\log_{10} \lambda_s} \log_{10} \lambda, \tag{26}$$

where r_{ta} is the turn-around radius, $\lambda = r/r_{ta}$, $\lambda_s = r_s/r_{ta} \simeq 0.3472$, where r_s is the radius of the accretion shock, and $V_{min} \simeq -1.433$ characterizes the inflow velocity of the gas just before passing through the accretion shock.

Contours of constant values of P_1 correspond to the values of constant projected accretion velocity. If at a radius r towards the source ($\theta = 0$), the accretion velocity is a fraction f of its maximum infall velocity, then contours of fixed P_1 will correspond to the surfaces

$$\lambda = \lambda_s^{f \sec(\theta)}, \tag{27}$$

extending over the angular range $0 \leq \theta \leq \arccos(f)$. The surface corresponding to $f = 0.5$ is shown in Fig. 5, with a maximum angle $\theta_{max} = 60^\circ$ and maximum radius $\lambda_0 = \lambda_s^f = 0.59$. The loci of constant P_1 correspond to arcing sheets. The exponential sensitivity of P_1 to v for $v_0/b_a \simeq x_1$ (see equation 25) ensures a surface of narrow width will dominate the 21-cm signal produced. Such a surface could be mistaken for the region of neutral hydrogen just outside an H II region surrounding a source of ionizing radiation. A varying gas temperature, and therefore varying b_a, in the accreting region will further complicate the signal. If $v_0/b_a \gg x_1$, then the entire solid hemisphere will be illuminated by the source (except for a thin circular wafer at $\theta \lesssim 90^\circ$).

A similar effect may apply to an expanding void. Since voids expand faster than the Hubble expansion, the peculiar velocity on the far side of a void from a distant source could redshift the received radiation into the line centre. A shell of direct scattering may then result even without including the reddening effects of radiative transfer within the void.

4 THE EVOLUTION OF THE WOUTHUYSEN-FIELD EFFECT IN DISCRETE OBJECTS

It was assumed for the solutions in Section 3 that the photons are able to achieve a steady state as they scatter within the absorbing system. In this section, we compute the time-scales required to establish a steady state by solving the time-dependent diffusion equation

$$\frac{\partial n(x,\tau)}{\partial \tau} = \frac{1}{2} \frac{\partial}{\partial x} \left[D(a,x) \frac{\partial n(x,\tau)}{\partial x} \right] + \tilde{S}(x), \tag{28}$$

where $\tau = t/t_s$ and $t_s = \Delta\nu_D/(n_1 \sigma c) \simeq 3.2 n_1^{-1} T_a^{1/2}$ s is the scattering time of the resonance line photons at line centre.

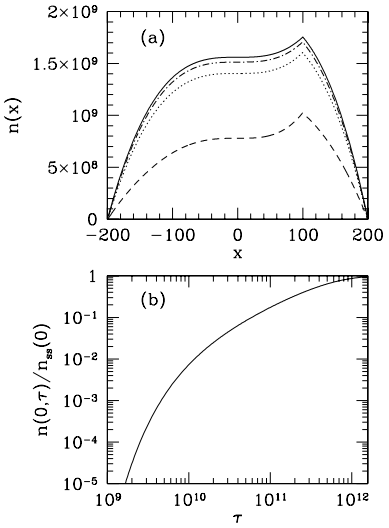

Figure 6. (a) Convergence of the time-dependent solution to the diffusion equation for a source $\tilde{S}(x) = \delta_D(x - x_{inj})$ with $x_{inj} = 100$, $x_{esc} = 200$ and $T_a = 100$ K. Shown are the steady-state photon frequency distribution, equation (18) (solid line) and the photon frequency distributions at the times their values at $x = 0$ take on 50 per cent (dashed line), 90 per cent (dotted line) and 97 per cent (dot-dashed line) of the steady-state value. (b) The evolution of the ratio of the photon frequency distribution at line centre ($x = 0$) to the steady-state value, as a function of time in units of the scattering time at line centre.

We solve equation (28) using a Crank–Nicholson scheme. We tested the scheme against the time-dependent solutions for a constant δ function source at line centre in an infinite homogeneous medium and a flat continuum source in the diffusion approximation (Rybicki & dell'Antonio 1994). The results applied to the source $\tilde{S}(x) = \delta_D(x - x_{inj})$ with $x_{inj} = 100$ and boundary condition $n(x) = 0$ for $|x| > x_{esc} = 200$ are shown in the upper panel of Fig. 6. The photon frequency distribution takes on the approximate shape of the final steady-state solution equation (18) as it converges towards it. The evolution of the photon frequency distribution at line centre ($x = 0$) is shown in the lower panel of Fig. 6. For sources that have been active only for a small fraction of the time required to achieve full convergence, the scattering rate may be negligibly small.

Dimensional analysis of equation (28) suggests the time to establish a steady state for photons injected at $x = x_{inj}$ is $\tau_{ss} \simeq 2x_{inj}^2/D(a, x_{inj}) \simeq (2\pi/a)x_{inj}^4 = (\pi/8a)x_{esc}^4 \simeq 8.3 T_a^{1/2} x_{esc}^4$ for $x_{inj} = x_{esc}/2$. The time for the photon distribution to converge to the steady-state value at $x = 0$ found from the numerical integration of equation (28) is shown in Fig. 7 for convergence to 50 and 90 per cent of the steady-state value, for a source $\tilde{S}(x) = \delta_D(x - x_{inj})$ with $x_{inj} = x_{esc}/2$ and $T_a = 100$ K. The convergence times scale like $\tau_{ss,50} \simeq 210 x_{esc}^4$ (50 per cent) and $\tau_{ss,90} \simeq 750\, x_{esc}^4$ (90 per cent), in good agreement with the expected behaviour.

5 DISCUSSION AND CONCLUSIONS

The role played by the WFE in decoupling the spin temperature of the neutral hydrogen from the CMB temperature depends most crucially on the scattering rate of Lyα photons. The spin temperature T_S is generally a weighted mean of the colour temperature T_α, kinetic temperature T_K of the gas and brightness temperature T_R of

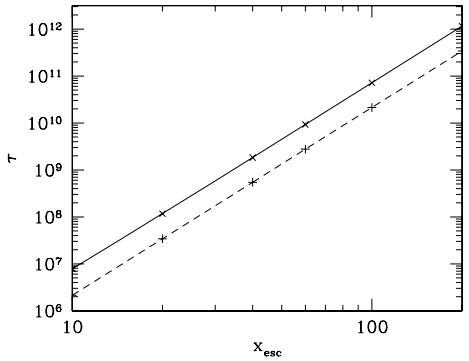

Figure 7. The convergence time in units of the scattering time at line centre for the photon frequency distribution with source $\tilde{S}(x) = \delta_D(x - x_{inj})$ having $x_{inj} = x_{esc}/2$ to reach 50 per cent (dashed line) and 90 per cent (solid line) of the steady-state value at $x = 0$. A temperature of $T_a = 100$ K is assumed.

any incident radiation (such as the CMB) at the 21-cm frequency,

$$T_S = \frac{T_R + y_\alpha T_\alpha + y_c T_K}{1 + y_\alpha + y_c}, \tag{29}$$

where

$$y_\alpha \equiv \frac{P_{10}}{A_{10}} \frac{T_*}{T_\alpha} \qquad \text{and} \qquad y_c \equiv \frac{C_{10}}{A_{10}} \frac{T_*}{T_K} \tag{30}$$

are the Lyα and collisional pumping efficiencies, respectively (Field 1958; Madau et al. 1997), $A_{10} = 2.85 \times 10^{-15}$ s^{-1} is the spontaneous decay rate of the 21-cm transition and $T_* \equiv h_P \nu_{10}/k_B$, where ν_{10} is the frequency of the 21-cm transition. Here, $P_{10} = 4P_1/27$ is the indirect de-excitation rate of the triplet hyperfine state induced by Lyα photon scattering. The colour temperature of the radiation field is the harmonic mean temperature $T_\alpha = 1/\langle T_u^{-1}(\nu)\rangle$, where $T_u(\nu) = -(h_P/k_B)(\mathrm{d} \ln \mathrm{u}_\nu/\mathrm{d}\nu)^{-1}$, weighted by $u_\nu\ \varphi_V(a, \nu)$ for an energy density u_ν of resonance line photons (Meiksin 2006). The coefficient C_{10} is the de-excitation rate of the triplet hyperfine state induced by atomic collisions.

For a Lyα scattering rate P_1 exceeding the critical thermalization rate

$$P_{th} = \frac{27 A_{10} T_{CMB}}{4 T_*} \simeq 6.8 \times 10^{-12}\ \mathrm{s}^{-1} \left(\frac{1+z}{9}\right), \tag{31}$$

where $T_{CMB} \simeq 2.73(1 + z)$ (Mather et al. 1994) is the CMB temperature, the spin temperature will be driven to the colour temperature in the absence of strong collisional de-excitation (Madau et al. 1997). The radiation field will typically rapidly thermalize with the neutral hydrogen, resulting in $T_\alpha \to T_K$ (Field 1959b; Meiksin 2006). The neutral hydrogen will then appear in either absorption or emission against the CMB, depending on whether T_K is below or above T_{CMB}, respectively.

Before the EoR, when the first radiation sources turn on at the EDA, regions around the sources may become visible through their 21-cm signature. Because the photons produced by a source, such as a QSO or star-forming galaxy, near the Lyα resonance will be scattered out of the line of sight over short distances, the scattering rate of Lyα photons will be much smaller than P_{th} except extremely near the source. Only photons emitted sufficiently bluewards of the Lyα resonance frequency will survive to any distant structures, where they will be received well in the blue Lorentz wing. If a structure has a sufficient optical depth in the wing to the photons received, it will trap them and rescatterings within the structure will allow the photons to diffuse in frequency across the resonance line. The radiation field may be built up in this way until it reaches a steady state in which the rate of incoming photons is balanced by the rate at which photons diffuse sufficiently far from the resonance line frequency to escape in the wings where the structure is optically thin. The resulting photon scattering rate in the diffusion approximation may greatly exceed the estimate $P_1(0)$ in the free-streaming limit, for which it is assumed that no resonance line photons emitted by the source have been scattered out of the line of sight before reaching the absorber.

We identify several factors, however, that may reduce the energy density of the resonance line photons from the steady-state diffusion approximation estimate for static structures:

(1) Internal expansion within the structure, characterized by the dimensionless expansion parameter γ, will redshift the photons into a red wing, where they will escape, on a time-scale much faster than the diffusion time, resulting in a much reduced energy density. In the diffusion approximation, the scattering rate will be reduced compared with the $\gamma = 0$ case by a factor of $(3a/\pi\gamma)/(x_{esc}^3 - x_{inj}^3)$ for $\gamma \gg \gamma_{crit} = 3a/(2\pi\, x_{esc}^3)$, where x_{esc} is the dimensionless escape frequency at which photons escape the structure and x_{inj} is the frequency at which photons are predominantly received from the source. Contraction within the structure may altogether prevent photons from diffusing across the resonance line frequency.

(2) The scattering rate may be reduced by atomic recoil. Estimating the magnitude of this effect, however, generally requires including non-trivial higher order terms in the recoil parameter ϵ than first order in the steady-state equation. We caution against introducing atomic recoils into Monte Carlo calculations and other steady-state solutions, as the results obtained may not be physically self-consistent if the solutions differ substantially from those obtained for $\epsilon = 0$.

(3) The time-scale to establish a steady state will typically exceed the duration of high star formation rates in galaxies or the lifetime of QSOs. As a consequence, the collision rate will be reduced by factors of tens to thousands as compared with the steady-state value.

As an illustration, consider the region around a bright QSO with specific luminosity at the Lyman edge of 10^{31} erg s^{-1} Hz^{-1} preheated by soft X-rays ahead of the ionization front to a mean temperature of $T_{IGM} \simeq 1800$ K at a distance of 10 Mpc (Madau et al. 1997). According to equation (4), $x_1 \simeq 200$ at $z = 8$ (assuming $h = 0.7$). A structure 250 kpc across with a moderate overdensity of three and internal temperature of $T_a \simeq 120$ K will have a neutral hydrogen column density of $N_{H\,I} \simeq 3 \times 10^{20}$ cm^{-2} and escape frequency $x_{esc} \simeq 200$, from equation (12). For a power-law spectrum $\nu^{-1.5}$, equation (10) gives for the Lyα collision rate in the free-streaming limit $P_1(0) \simeq 8.7 \times 10^{-13}$ s^{-1}, about an order of magnitude smaller than the thermalization rate P_{th}. The steady-state value from equation (19) then gives $P_{1,ss} \simeq 10^{-8}$ s^{-1}, well in excess of P_{th}. The time to establish a steady state, however, is long. The scattering time of Lyα photons in the structure is about $t_s \simeq 8.5 \times 10^4$ s. According to Fig. 7, the time for the radiation field to achieve a steady state is then about 10^{17} s, or 3 Gyr, greatly exceeding the expected lifetime of the QSO. If the QSO had illuminated the structure for as long as 0.1 Gyr, according to Fig. 6 the steady-state value must be reduced by a factor of 0.05. The resulting scattering rate will still exceed P_{th}. If the system has a peculiar velocity away from the QSO, the rate could be quite different. Equation (24) shows that a peculiar velocity of 140 km s^{-1}, a plausible value, would shift the peak of the radiation from the source received by the structure to the resonance line frequency. The radiation field would then rapidly reach its steady-state value, and $P_{1,ss}$ would greatly exceed P_{th}.

A much more overdense structure at the same distance from the QSO would be able to achieve the steady-state scattering rate. For example, a virialized structure 35 kpc across with an overdensity of 200 and temperature $T_a \simeq 1000$ K would have a neutral hydrogen column density of 3×10^{21} cm^{-2} and $x_{esc} \simeq 220$. The time for the radiation field to reach a steady state would then be about 0.2 Gyr, a plausible lifetime for the QSO.

By contrast, it may be difficult to achieve a steady state in a void. For an IGM temperature $T_{IGM} \simeq 100$ K, $x_1 = 825$ at $z = 8$. A region 3 Mpc across with a temperature of $T_a = 10$ K, and underdense by a factor of 3 will have a neutral hydrogen column density of 4×10^{20} cm^{-2}, $x_{esc} \simeq 800$ and a scattering time at line centre of $t_s \simeq 2.2 \times 10^5$ s. The time to reach a steady state is then 2100 Gyr. Even if the void is illuminated for as long as the age of the Universe, the radiation field will be negligibly small compared with its steady-state value. Since the void will expand, however, the incident radiation will be redshifted across the resonance line. Rybicki & dell'Antonio (1994) estimate a characteristic time for redshifting to dominate diffusion in an infinite homogeneous medium to be $\tau_\gamma \simeq (a/\gamma^4)^{1/3}$. Voids expand somewhat faster than the mean Hubble expansion. Adopting the Hubble constant at $z = 8$ for $h = 0.7$, $\gamma \simeq 5 \times 10^{-6}$. A steady state should be established for $t \gg \tau_\gamma t_s \simeq 2 \times 10^4$ yr, and the steady-state scattering rate will then match the free-streaming value, with $P_{l,ss}/P_l(0) \simeq a/(\pi\gamma x_1) \simeq 1$, which may be adequate for producing a 21-cm signature in the presence of sufficient sources.

The examples above show that the effect of peculiar motions may lead to an enhancement in the Lyα scattering rate over the free-streaming limit and produce the required decoupling of T_S from T_{CMB}. Even if the scattering rate is inadequate for inducing decoupling throughout most of the structure, it may be adequate along narrow loci within which the velocity field either permits the resonance line photons to accumulate near the resonance line frequency or shifts the resonance line frequency of the absorber to matching the peak frequency of the incident radiation field from the source as filtered through the IGM. We presented an example of an accreting halo which produces a 21-cm signature along a curved surface for which the impinging photons are received at the resonance line frequency due to the infall velocity of the accreting gas. Such a curved structure could be mistaken for a rim of neutral gas outside an H II region in radio maps of the IGM. Similar curved surfaces may form on the far side of voids from a distant source.

As a consequence of the above effects, the 21-cm signature of the IGM will not simply trace the density structure of the IGM, but will trace the peculiar velocity structure as well. We have not considered multiple sources. In the presence of a large number of nearby sources, a greater fraction of the gas will be able to match the incident radiation field through their peculiar motions. In addition, the escaping radiation from the absorbers will contribute to the ambient radiation field. In due course, a metagalactic diffuse radiation field may grow sufficiently strong to ensure that the WFE is capable of decoupling the spin temperature from the CMB temperature throughout the IGM, and so ensure the production of a 21-cm signature everywhere. The effects described here suggest that in the early stages, before any such metagalactic field has been established (and it has yet to be demonstrated that such a field will be established), the 21-cm signatures produced at the EDA, and possibly extending into the EoR, may only be interpreted with a thorough understanding of the evolution of the energy density of resonance line photons within a clumpy medium, including the effects of peculiar motions.

ACKNOWLEDGMENT

JH thanks STFC for a postgraduate fellowship.

REFERENCES

Adams T. F., 1972, ApJ, 174, 439
Basko M. M., 1981, Astrophysics, 17, 69
Becker R. H. et al., 2001, AJ, 122, 2850
Bertschinger E., 1985, ApJS, 58, 39
Chen X., Miralda-Escudé J., 2004, ApJ, 602, 1
Chuzhoy L., Zheng Z., 2007, ApJ, 670, 912
Fan X., Carilli C. L., Keating B., 2006, ARA&A, 44, 415
Field G. B., 1958, Proc. I.R.E., 46, 240
Field G. B., 1959a, ApJ, 129, 536
Field G. B., 1959b, ApJ, 129, 551
Furlanetto S. R., Oh S. P., Briggs F. H., 2006, Phys. Rep., 433, 181
Gnedin N. Y., Shaver P. A., 2004, ApJ, 608, 611
Gunn J. E., Peterson B. A., 1965, ApJ, 142, 1633
Harrington J. P., 1973, MNRAS, 162, 43
Hogan C. J., Rees M. J., 1979, MNRAS, 188, 791
Loeb A., Barkana R., 2001, ARA&A, 39, 19
Loeb A., Rybicki G. B., 1999, ApJ, 524, 527
Madau P., Meiksin A., Rees M. J., 1997, ApJ, 475, 429
Mather J. C. et al., 1994, ApJ, 420, 439
Meiksin A., 2006, MNRAS, 370, 2025
Mihalas D., 1978, Stellar Atmospheres, 2nd edn. Freeman & Co., San Francisco, p. 650
Neufeld D. A., 1990, ApJ, 350, 216
O'Meara J. M., Burles S., Prochaska J. X., Prochter G. E., Bernstein R. A., Burgess K. M., 2006, ApJ, 649, L61, preprint (arXiv:astro-ph/0608302)
Osterbrock D. E., 1962, ApJ, 135, 195
Pierleoni M., Maselli A., Ciardi B., 2008, MNRAS, in press
Rybicki G. B., dell'Antonio I. P., 1994, ApJ, 427, 603
Scott D., Rees M. J., 1990, MNRAS, 247, 510
Semelin B., Combes F., Baek S., 2007, A&A, 474, 365
Spergel D. N. et al., 2007, ApJS, 170, 377
Tozzi P., Madau P., Meiksin A., Rees M. J., 2000, ApJ, 528, 597
Wouthuysen S. A., 1952, AJ, 57, 31
Zhang Y., Meiksin A., Anninos P., Norman M. L., 1998, ApJ, 495, 63

APPENDIX A: OPTICAL DEPTH THROUGH DOPPLER CORE

Radiation from a source at z_S received at z with frequency ν in the range $\nu_0[(1+z)/(1+z_S)] < \nu < \nu_0$, where ν_0 is the resonance line frequency, would have passed through the resonance line frequency en route to the absorber. To estimate the optical depth of the IGM at these frequencies, it is convenient to approximate the Voigt line profile as

$$\phi_V(a,x) = \pi^{-1/2}\exp(-x^2); \qquad -x_m < x < x_m$$
$$= \frac{a}{\pi x^2}; \qquad |x| > x_m, \tag{A1}$$

where x_m is the value of $x = (\nu - \nu_0)/\Delta\nu_D$ at which the two approximations match. For $T = 10$, 100 and 1000 K, the values of x_m are 2.58, 2.83 and 3.05, respectively.

A photon of frequency ν at z will have $x = \pm x_m$ at the redshift $z_m^{(\pm)}$, given by

$$\frac{\nu}{\nu_0}\frac{1+z_m^{(\pm)}}{1+z} = 1 \pm x_m\frac{b}{c}, \tag{A2}$$

where $b = (2k_BT_{IGM}/m_H)^{1/2}$ is the Doppler parameter of the IGM at temperature T_{IGM}, assumed constant. (In principle, a turbulent velocity component may be added in quadrature.) The optical depth in

equation (1) may then be expressed as a sum of three contributions, corresponding to the ranges $x < -x_m$, $-x_m < x < x_m$ and $x > x_m$,

$$\tau_\nu = \frac{\sigma a}{\pi\Delta\nu_{\rm D}}\int_z^{z_m^{(-)}} {\rm d}z'\,\frac{{\rm d}l_p}{{\rm d}z'}n_{\rm l}(z')\frac{(\Delta\nu_{\rm D})^2}{\left(\nu\frac{1+z'}{1+z}-\nu_0\right)^2} + \frac{\sigma}{\pi^{1/2}\Delta\nu_{\rm D}}\int_{z_m^{(-)}}^{z_m^{(+)}} {\rm d}z'\,\frac{{\rm d}l_p}{{\rm d}z'}n_{\rm l}(z')\exp\left[-\left(\frac{\nu\frac{1+z'}{1+z}-\nu_0}{\Delta\nu_{\rm D}}\right)^2\right] + \frac{\sigma a}{\pi\Delta\nu_{\rm D}}\int_{z_m^{(+)}}^{z_{\rm S}} {\rm d}z'\,\frac{{\rm d}l_p}{{\rm d}z'}n_{\rm l}(z')\frac{(\Delta\nu_{\rm D})^2}{\left(\nu\frac{1+z'}{1+z}-\nu_0\right)^2}. \quad \text{(A3)}$$

The first and third terms are similar to equation (2). The dominant term is the second, representing scattering through the line core. Setting $u = \{[\nu(1+z')/(1+z)-\nu_0]/\Delta\nu_{\rm D}\}^2$, and assuming $b/c \ll 1$ within the integrand, gives for this contribution

$$\tau_\nu^{\rm core} \simeq \frac{1}{\pi^{1/2}}\frac{\sigma cn(0)}{H_0\Omega_{\rm m}^{1/2}}(1+z)^{3/2}\nu_0^{1/2}\nu^{-3/2}\gamma\left(\frac{1}{2},x_m^2\right) \simeq 8000h^{-1}(1+z)^{3/2}y^{-3/2}\gamma\left(\frac{1}{2},x_m^2\right), \quad \text{(A4)}$$

where $y = \nu/\nu_0$, $\gamma(t,x) = \int_0^x {\rm d}u u^{t-1}\exp(-u)$ is an incomplete gamma function, and $\Omega_{\rm m} = 0.3$ and $\Omega_{\rm b}h^2 = 0.022$ are assumed. This will in general ensure that essentially no flux from the source is received in the frequency range $\nu_0(1+z)/(1+z_{\rm S}) < \nu < \nu_0$. This is the Gunn–Peterson effect.

APPENDIX B: SLAB SOLUTION

The diffusion equation for the transfer of radiation through a static slab in the Eddington approximation is given by Harrington (1973) as

$$\frac{\partial^2 n_x(\tau,\sigma)}{\partial\tau^2}+\frac{\partial^2 n_x(\tau,\sigma)}{\partial\sigma^2} = -3\phi_{\rm V}^2(a,x)\frac{G(\tau)}{4\pi}, \simeq -6^{1/2}\delta_{\rm D}(\sigma)\frac{G(\tau)}{4\pi}, \quad \text{(B1)}$$

for a spectrally flat source $G(\tau)$, in the limit $\phi_{\rm V}(a,x) \simeq a/(\pi x^2)$. Here, σ is related to x through ${\rm d}x/{\rm d}\sigma = (3/2)^{1/2}\,\phi_{\rm V}(a,x)$ and $\tau = \tau_\nu/\phi_{\rm V}(a,x)$ is the mean optical depth vertically through the slab. The photon number density $n(x)$ is expressed as $n_x(\sigma)$. The last line in equation (B1) follows from approximating $3\phi_{\rm V}^2(a,x)$ as a Dirac δ function, $6^{1/2}\,\delta_{\rm D}(\sigma)$, where the coefficient preserves the normalization. The boundary conditions assumed are

$$\left.\frac{\partial n_x(\tau,\sigma)}{\partial\tau}\right|_{\pm B} = \mp\frac{3}{2}\phi_{\rm V}(a,x)n_x(B,\sigma) \quad \text{(B2)}$$

and

$$n_x(\tau,\sigma)\to 0 \quad \text{for} \quad \sigma\to\pm\infty. \quad \text{(B3)}$$

For a uniformly distributed source of unit strength, Harrington (1973) takes $G = 1/(2B)$, where $-B < \tau < B$ describes the vertical extent of the slab. In terms of the total optical depth at line centre, $\tau_0 = 2B\phi_{\rm V}(a,0) = 2B/\pi^{1/2}$, the source becomes $G = \pi^{-1/2}/\tau_0$. The solution at the centre of the slab is

$$n_x(0,x) = \frac{6^{1/2}}{2\pi^3}S\left(\exp\left[-2^{1/2}\left(\frac{\pi}{3}\right)^{3/2}\frac{|x|^3}{a\tau_0}\right]\right), \quad \text{(B4)}$$

where the function $S(z) = z - z^3/3^2 + z^5/5^2 - +\ldots \simeq z$ for $0 < z < 1$.

The diffusion approximation equation (14) transforms to

$$\frac{{\rm d}^2 n_x(\sigma)}{{\rm d}\sigma^2} = -6^{1/2}A\delta_{\rm D}(\sigma), \quad \text{(B5)}$$

for a source $\tilde{S}(x) = A\delta_{\rm D}(x)$ and adopting $D(a,x) = \phi_{\rm V}(a,x)$. Identifying $A = G/(4\pi) = 1/(4\pi^{3/2}\tau_0)$ reproduces equation (B1) with the τ-dependence suppressed. Expressing $x_{\rm esc} = x_*(a\tau_0)^{1/3}$, the solution equation (18) becomes

$$n_x(x) = \frac{x_*^3}{12\pi^{1/2}}\left(1-\frac{|x|^3}{x_*^3 a\tau_0}\right) \qquad (|x|\le x_{\rm esc}), \quad \text{(B6)}$$

for $x_{\rm inj} = 0$. Noting $S(1) \simeq 0.92$, equating the values of equations (B4) and (B6) at $x = 0$ gives $x_* \simeq 0.92$. The two profiles are very similar, with equation (B4) forming an exponential tail with a cut-off at $x \gtrsim 0.87(a\tau_0)^{1/3} \simeq 0.95x_{\rm esc}$.

This paper has been typeset from a TEX/LATEX file prepared by the author.